PCCP

PAPER

View Article Online
View Journal | View Issue

Cite this: *Phys. Chem. Chem. Phys.*, 2026, **28**, 7774

Broadband cross polarization for ultra-wideline magic-angle spinning NMR†

James J. Kimball, [ab] Sophia Keil, [c] Max Bußkamp,[c] Adam R. Altenhof, [ab] Michael Ryan Hansen *[cd] and Robert W. Schurko *[ab]

Over the past decade, there has been a sustained interest in using frequency-swept (FS) pulses for the efficient acquisition of wideline and ultra-wideline (UW) NMR powder patterns. Such experiments are typically conducted under static conditions, employing both direct- and indirect-excitation methods (*i.e.*, WCPMG and BRAIN-CP/WCPMG, respectively). Recently, Koppe *et al.* demonstrated that the WCPMG pulse sequence can be used to efficiently acquire wideline and UW NMR spectra with spinning sideband (SSB) manifolds under magic-angle spinning (MAS) conditions, capitalizing on the increased signal-to-noise ratios (SNR) afforded by MAS. To date, there have been only a few instances of broadband cross-polarization (CP) experiments using FS pulses under MAS conditions and no applications to systems exhibiting wideline and/or ultra-wideline powder patterns, despite the clear advantages these experiments could offer. Herein, we demonstrate that FS pulses selectively applied to a single sideband of the *S* spin can be used for efficient ^{1}H-*S* polarization transfer to *S* = 1/2 nuclides with large anisotropic chemical shift interactions at slow to moderate MAS rates. The Hartmann–Hahn matching conditions in BRAIN-CP/WCPMG-MAS experiments bear similarity to those of standard CP sequences, yet operate over UW frequency ranges and only require low-amplitude RF pulses on the *S* channel. Crucial to the success of the BRAIN-CP/WCPMG-MAS experiment is careful calibration of the RF amplitude, transmitter offset, and effective frequency sweep of the FS pulse applied to the *S* spins at a given MAS rate. Thus, by means of numerical simulations and experimental testing, we provide recommendations for the parameterization and setup of BRAIN-CP/WCPMG-MAS experiments for their most efficient use. Results showcasing the capability of the BRAIN-CP/WCPMG-MAS pulse sequence are presented, including applications to ^{119}Sn, ^{195}Pt, and ^{103}Rh NMR.

Received 12th October 2025,
Accepted 9th February 2026

DOI: 10.1039/d5cp03931b

rsc.li/pccp

1. Introduction

In recent years, the increasing availability of high magnetic fields has posed a significant challenge for solid-state NMR (SSNMR) of nuclides affected by strong chemical shift anisotropy (CSA), as their powder pattern breadths scale proportionally with the applied magnetic field strength, B_0. In instances of SSNMR spectra with ultra-wideline (UW) powder patterns (*i.e.*, those with breadths surpassing 250 kHz), the effectiveness of traditional pulsed NMR methods is compromised due to the inability to manipulate spin polarization across large frequency bandwidths using rectangular pulses and conventional probes.[1] Nevertheless, acquisition of such SSNMR spectra is not insurmountable, as numerous pulse sequences have been designed for this very purpose.[2–5]

At the heart of these methods is the use of frequency-swept (FS) pulses, which feature time-dependent phases with the optional addition of modulated amplitudes.[6,7] These pulses have been used extensively for a wide variety of purposes, including but not limited to excitation, refocusing, and polarization transfer – all of which are crucial building blocks for many commonly used techniques in NMR.[8–10] Of the wide variety of FS pulses available, wideband, uniform rate, smooth truncation (WURST) pulses featuring linear frequency sweeps have found the most success in UW NMR experiments.[11,12] The most prevalent example is the WURST-CPMG (WCPMG) sequence, wherein WURST pulses are used for direct excitation (DE) in CPMG-style experiments under both static and MAS conditions.[13–15] For indirect excitation (*i.e.*, ^{1}H → S cross polarization, CP) experiments, WURST pulses are used in the framework of the broadband adiabatic inversion cross-polarization

[a] *Department of Chemistry & Biochemistry, Florida State University, Tallahassee, FL 32306, USA. E-mail: rschurko@fsu.edu*
[b] *National High Magnetic Field Laboratory, Tallahassee, FL 32310, USA*
[c] *Institute for Physical Chemistry, University of Münster, Münster, DE-48149, Germany. E-mail: mhansen@uni-muenster.de*
[d] *Center for Multiscale Theory and Computation (CMTC), University of Münster, Münster, DE-48149, Germany*

† This work is dedicated to the memory of Professor Robert W. Schurko, whose thoughtful insight and guidance were instrumental to the success of this project.

(BRAIN-CP) sequence, enabling efficient CP across bandwidths well into the UW regime.[16] BRAIN-CP has been thoroughly explored in applications to static samples;[17,18] however, the use of FS pulses for broadband CP under MAS conditions has been limited to date,[19–21] and there exist no examples of its application for the acquisition of UW NMR spectra under MAS conditions without the assistance of techniques such as acquisition of a variable offset cumulative spectrum (VOCS), wherein the transmitter is ''frequency stepped'' across the pattern breadth.[22,23]

The complex behavior of FS pulses under MAS has likely hindered their widespread application; however, this is not unexplored territory. Pell and coworkers demonstrated the use of WURST pulses for broadband inversion of spin polarization under MAS.[24–28] In such experiments, the phase modulation of the pulse is set such that the effective frequency sweeps across just one spinning sideband (SSB), yet inversion of the entire sideband manifold is observed. WURST applied in this way are referred to as single-sideband selective adiabatic pulses (S^3APs) and their performance in terms of spin locking and adiabatic inversion hinges upon satisfaction of the following experimental protocols: (i) the sweep width (Δ, as determined by the phase modulation) is matched to the MAS rate ($\omega_{rot} = 2\pi\nu_{rot}$, *i.e.*, $\Delta = \nu_{rot}$)[25] and (ii) the offset frequency ($\Omega_S = \omega_{0,S} - \omega_{Tx,S}$, where $\omega_{0,S}$ is the Larmor frequency and $\omega_{Tx,S}$ is the time-independent transmitter frequency) is set such that the frequency sweep centered at a transmitter frequency of $\omega_{Tx,S}$ passes through the resonance frequency of a single SSB.[27] Also of importance is the pulse amplitude ($\omega_{1,S} = 2\pi\nu_{1,S}$), which has direct implications on the adiabaticity of the S^3AP. Ideally, the condition $|\nu_{1,S}| \ll |\nu_{rot}|$ is in place;[26] yet, efficient inversion across UW frequency ranges has been also reported in the more intermediate regime of $|\nu_{1,S}| \approx |\nu_{rot}|$.[28]

In this work, we demonstrate the implementation of S^3APs for CP in a manner not unlike that of the BRAIN-CP sequence in combination with WCPMG incremented echo acquisition[14] (hence the name BRAIN-CP/WCPMG-MAS). The S^3AP is used for fulfillment of the HH matching conditions and subsequent spin locking of the magnetization produced from broadband CP, and culminates with the storage of magnetization along the *z*-axis. The principles outlined by Pell and coauthors are used in the theoretical description of the BRAIN-CP/WCPMG-MAS experiment. Hartmann–Hahn (HH) matching conditions are derived using a combination of analytical equations, simulated experiments, and experimental measurements. Parameters crucial to the success of the BRAIN-CP/WCPMG-MAS sequence, which include the transmitter offset, spin locking amplitude, and phase modulation of the S^3AP, are addressed in detail. Uniform polarization transfer across bandwidths surpassing 1 MHz is demonstrated, showcasing the capability of a properly optimized BRAIN-CP/WCPMG-MAS sequence. A variety of experimental results are used to illustrate the potential of BRAIN-CP/WCPMG-MAS for significant reduction in the experimental times required to obtain spectra of both wideline (*ca.* 50–250 kHz in breadth) and UW SSB manifolds of spin-1/2 nuclides, compared to analogous static and/or direct-excitation experiments.

2. Experimental methods

2.1 Samples

Dibutyltin oxide [DBTO, Sigma Aldrich], cisplatin [$Pt(NH_3)_2Cl_2$, Thermo Fisher], and chloro(1,5-cylcooctadiene)rhodium(I) dimer [$Rh_2Cl_2(COD)_2$, Strem] were purchased from the listed sources and used in all subsequent NMR experiments without further purification. The identities and purities of the samples were verified through comparisons with previously reported SSNMR spectra and PXRD patterns. The novel [Sn(HPDABA)]Cl_2 (HPDABA = 2-hydroxy-4-(propan-2-ylideneamino)benzoic acid) cocrystal was prepared mechanochemically *via* ball milling (see SI for the synthetic procedure). All samples were ground into fine powders on the benchtop under ambient conditions and were packed into 3.2 mm (for $\nu_{rot} \leq 15$ kHz) and 2.5 mm (for $\nu_{rot} > 15$ kHz) zirconium NMR rotors.

2.2 SSNMR spectroscopy

Bruker Avance NEO consoles were used for all experiments. ^{1}H–^{119}Sn NMR spectra were acquired using a 14.1 T Magnex/Bruker [ν_0 (^{1}H) = 600 MHz] wide bore magnet with a resonance frequency of ν_0 (^{119}Sn) = 223.744 MHz. ^{1}H–^{195}Pt NMR experiments were conducted using a 11.7 T Bruker [ν_0 (^{1}H) = 500 MHz] wide bore magnet with ν_0 (^{195}Pt) = 106.700 MHz. ^{1}H–^{103}Rh NMR experiments were conducted using a 21.1 T [ν_0 (^{1}H) = 900 MHz] home-built ultra-wide bore magnet with ν_0 (^{103}Rh) = 28.678 MHz. Home-built 3.2 mm triple-resonance (HXY) and 3.2 mm double-resonance (HX) probes were used for experiments at 14.1 T and 21.1 T, respectively. A 2.5 mm triple resonance (HXY) probe was used for experiments at 11.7 T. A Bruker MAS3 unit was used for all MAS NMR experiments with ν_{rot} set between 10 and 25 kHz. The magic angle of the NMR probes was calibrated to 54.74° by maximizing the number of rotational echoes observed in the ^{79}Br FID of KBr[29] or by minimizing the linewidth of the SSBs in the ^{23}Na MAS NMR spectrum of $NaNO_3$.[30]

Pulse width calibrations for all *S* nuclides (excluding those for ^{195}Pt which were performed with a Bloch decay) were performed under static conditions by arraying the width of an excitation pulse (τ_{cal}) inserted between the contact pulse and the first refocusing pulse in a CP/CPMG experiment (see SI for the pulse sequence, Scheme S1). In each case, the transmitter frequency was tuned to a discontinuity of high signal intensity in the powder pattern and care was taken to interpret the resulting nutation curve according to the on-resonance signal only. ^{119}Sn chemical shifts were referenced to neat $Sn(CH_3)_4$ with δ_{iso} = 0 ppm using SnO(s) as a secondary reference ($\delta_{22} = \delta_{33}$ = 121.3 ppm and δ_{11} = 866.7 ppm, where δ_{11} and δ_{22} represent the largest principal components (lowest shielding) of the chemical shielding tensor using the standard convention).[31] ^{195}Pt chemical shifts were referenced to 1.0 M K_2PtCl_6(aq) with δ_{iso} = 0 ppm. ^{103}Rh chemical shifts were referenced such that $\delta(^{103}Rh) = 0$ ppm using a frequency ratio of Ξ = 3.16% relative to the ^{1}H resonance frequency of TMS(*l*).[32]

Calibrated spin-locking fields applied to the *S* and *I* spins, $\nu_{1,S}$ and $\nu_{1,I}$, were set as $\nu_{1,S}$ = 5–25 kHz and $\nu_{1,I}$ = 5–50 kHz for

all experiments in order to fulfill the BRAIN-CP/WCPMG-MAS HH matching conditions (see Section 3.3). These were determined as the ratio of RF powers on the S and I channels yielding spectra with patterns of the highest signal intensity and overall pattern uniformity. In all experiments, the condition $\Delta = \nu_{1,S} = \nu_{rot}$ was fulfilled in order to achieve broadband adiabatic spin locking, where Δ is the sweep width of the contact pulse as determined by the phase modulation, and ν_{rot} is the MAS rate. The contact pulse lengths, τ_{CT}, are on the order of milliseconds, with the exact experimental values determined from the relative magnitudes of the approximate heteronuclear dipolar couplings and SSB manifold breadths, as is conventionally done in the optimization of CP-type experiments.[18,33]

Rotor synchronization of excitation and refocusing WURST pulses during the CPMG train (Scheme 1) was achieved by ensuring that the condition $2M\tau_{rot} = 2\tau_2 + \tau_{ref} + \tau_{SE}$ was satisfied, where $2M$, τ_{rot}, τ_2, τ_{ref}, and τ_{SE} are the number of rotor periods per CPMG cycle, the rotor period, the dead time, the refocusing pulse width, and the length of the spin echo, respectively and M is an integer.[34] In order to maximize signal intensity, the amplitudes of the excitation and refocusing WURST pulses were adjusted to satisfy the condition $\nu_{exc/ref} = \frac{0.26 \times R_{exc/ref}{}^{1/2}}{(S+1/2)} + c$, where c is an experimentally determined constant, $R_{exc/ref} = \Delta_{exc/ref}/\tau_{exc/ref}$ is the sweep rate of the WURST excitation and refocusing pulses, $\Delta_{exc/ref}$ is the sweep width, and $\tau_{exc/ref}$ is the pulse length.[35,36] $R_{exc/ref}$ was set to satisfy the condition $x \geq 3$, where $x = R_{exc/ref}/(\Omega_{SSB}\cdot\nu_{rot})$ and Ω_{SSB} is the breadth (expressed in Hz) of the SSB manifold that is traversed by the effective frequency sweep over the course of one rotor period.[14] As described by Koppe and coworkers,[14] conditions of $x \geq 10$ result in more efficient excitation and refocusing; however, for SSB manifolds in UW NMR spectra where Ω_{SSB} is much larger, higher R values are required to meet these conditions, thereby necessitating higher amplitudes of $\nu_{exc/ref}$. In some cases, this is unachievable due to probe power limitations (*e.g.*, in ^{1}H–^{103}Rh experiments). All BRAIN-CP/WCPMG-MAS experiments required optimization of the transmitter offset of the pulse applied to the S spins (Ω_S). This was accomplished by arraying Ω_S and choosing the value resulting in the signal of highest intensity. The need for initial optimization of Ω_S is less essential in cases where δ_{iso} is known, as a value of Ω_S around $\delta_{iso} \pm \omega_{rot}/2$ (such that the transmitter is tuned adjacent to the isotropic shift) can be used as a starting point (see Section 3.3). It is nevertheless recommended to optimize this parameter after adjusting the HH matching conditions.

A full list of all BRAIN-CP/WCPMG-MAS and WCPMG-MAS parameters is given in Tables S1 and S2. All spectra were acquired using TPPM ^{1}H decoupling with RF fields between 30–50 kHz, excluding the ^{195}Pt spectra of cisplatin which were recorded using swept-frequency TPPM decoupling with an RF amplitude of 83 kHz. Direct-excitation (DE) schemes employ the eight-step phase cycling scheme used by Bhattacharyya and Frydman[37] and CP schemes use the sixteen-step phase cycling scheme used by Larsen and co-workers.[38] All pulse sequences described herein are available upon request or at https://github.com/rschurko.

2.3 Spectral processing and simulations

All data sets were processed in MATLAB *via* multiplication of each echo with a multi-peak Gaussian function, coaddition of echoes, fast-Fourier transform, and magnitude calculation (*i.e.*, spectra are not phased) using a custom-written code (available on request). Numerical simulations, performed with both the SIMPSON 4.1.1[39] open source software package and a custom written simulation package in MATLAB R2023b, were used to monitor spin dynamics. An *IS* spin system ($I = {}^{1}$H, $S = \frac{1}{2}$) was used, with an axially symmetrical CS tensor for the S spin where δ_{iso} = 0 ppm, Ω_{CS} = either 675 or 1350 ppm (indicated in each case), and $\kappa = -1$, using the Herzfeld–Berger convention (or δ_{iso} = 0 ppm, $\Delta\delta$ = either 450 or 900 ppm (indicated in each case), and η = 0, using the Haeberlen convention).[40] The heteronuclear dipolar coupling constant is given by

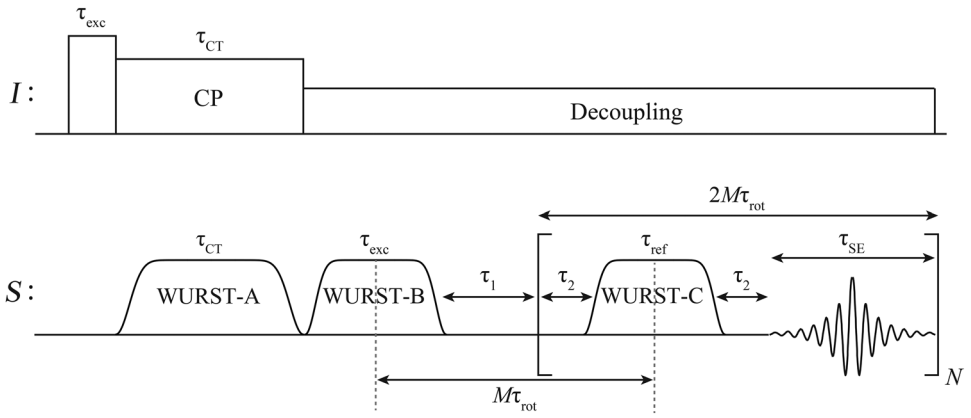

Scheme 1 Schematic representation of the BRAIN-CP/WCPMG-MAS pulse sequence. Rotor synchronization is achieved when the duration of a single CPMG cycle, defined as the total time of a single refocusing pulse along with the two associated ring-down delays and the subsequent windowed spin-echo acquisition period, is an integer multiple of the rotor period (*i.e.*, $2M\tau_{rot} = 2\tau_2 + \tau_{ref} + \tau_{SE}$ is satisfied). Here M is an integer and N is the number of CPMG loops. See main text for full description of all variables.

$b_D^{IS} = \gamma_I\gamma_S r_{IS}^{-3}(\hbar 2\pi)(\mu_0/4\pi)$ and the corresponding dipolar frequency is given by $\omega_D^{IS} = \frac{b_D^{IS}}{2}(3\cos\theta^2 - 1) = 2\pi\nu_D^{IS}$ where θ describes the angle between the principle axis system (PAS) of the heteronuclear dipolar tensor and the rotor axis. In all cases, $b_D^{IS}/2\pi$ and θ were set to 4 kHz and 45°, respectively. All simulations were conducted using a magnetic field strength of 14.1 T.

Throughout this work, we use the term isochromats to refer to groups of nuclear spins that precess at identical rates. Isochromats are distinguished by their orientations, defined by the angles α and β, where α is the azimuthal angle and β describes the relative orientation of the PAS for the chemical shift tensor and the unique axis of the MAS frame. In cases of axially symmetric CS tensors, the former angle is irrelevant and thus isochromats can be described completely by the angle β. Assuming a homogeneous $\mathbf{B}_0$, different isochromats thus represent unique resonance frequencies which collectively comprise a SSB manifold under MAS. For simplicity, axially symmetric CS tensors are used in all ensuing simulations unless otherwise denoted. Powder averaging is accomplished using the REPULSION scheme,[41] with the number of orientations indicated in each case. Calculations were performed on a MacBook Pro operating on macOS 14.1.1 with an Apple M1 Pro chip and on NMRBox virtual machines.[42]

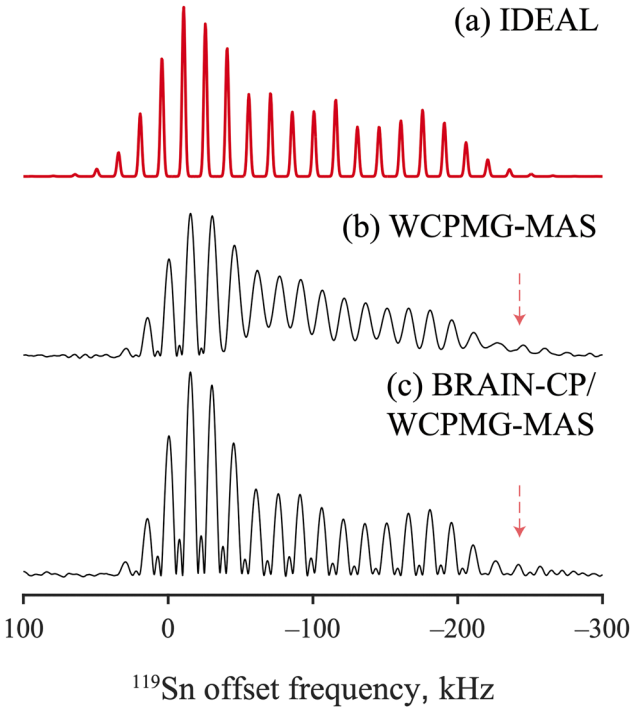

Fig. 1 (a) Simulated and (b and c) experimental ^{119}Sn MAS NMR spectra of [Sn(HPDABA)]Cl_2 acquired at 14.1 T using (b) WCPMG/MAS and (c) BRAIN-CP/WCPMG-MAS at a spinning rate of ν_{rot} = 15 kHz. $\Omega_S/2\pi$ is indicated by the dotted red arrows.

3. Protocols

3.1 A first example: wideline ^{1}H–^{119}Sn BRAIN-CP MAS NMR

The novel co-crystal [Sn(HPDABA)]Cl_2 was chosen as a test case due to its favorable NMR properties for spectral acquisition using BRAIN-CP/WCPMG-MAS. Its large ^{119}Sn CSA (Ω_{CS} = 760 ppm, *ca.* 200 kHz in breadth at 14.1 T) and long $T_1(^{119}Sn)$ time constant (estimated 40 s from an optimized recycle delay of 200 s) render DE methods impractical for the acquisition of ^{119}Sn SSNMR spectra. However, the much shorter $T_1(^1H)$ time constant (estimated from an optimized recycle delay of 5 s), in addition to ^{1}H–^{119}Sn heteronuclear dipolar coupling constants of moderate magnitude, set the stage for efficient CP experiments.

The ^{1}H–^{119}Sn BRAIN-CP/WCPMG-MAS spectrum of [Sn(HPDABA)]Cl_2 was acquired in just 8 minutes at 14.1 T and MAS rate of ν_{rot} = 15 kHz (Fig. 1c), revealing a SSB manifold closely resembling the simulated ideal spectrum (Fig. 1a). Spectral acquisition *via* BRAIN-CP/WCPMG-MAS (Fig. 1c) is more efficient than with WCPMG-MAS (*i.e.*, by more than an order of magnitude, 8 minutes *vs.* 3.5 hours; Fig. 1b, see Scheme S2 for the pulse sequence) for two reasons: (i) the ^{1}H–^{119}Sn BRAIN-CP/WCPMG-MAS is efficient, resulting in enhanced signal intensity; and (ii) $T_1(^1H)$ is much shorter than $T_1(^{119}Sn)$, allowing for shorter recycle delays. The spectral distortions manifesting as low intensity peaks between the SSBs are from the use of short τ_{SE} values (Fig. S1, see Section 3.4) in an effort to maximize SNR.

In the sections that follow, we demonstrate that ^{1}H-*S* BRAIN-CP/WCPMG-MAS spectra of similar quality can be acquired after optimization of several experimental parameters: the transmitter offset ($\Omega_S = \omega_{0,S} - \omega_{Tx,S}$, Section 3.2), the RF amplitudes on the ^{1}H and *S* channels ($\omega_{1,I} = 2\pi\cdot\nu_{1,I}$ and $\omega_{1,S} = 2\pi\cdot\nu_{1,S}$, respectively, Section 3.3), and matching of the sweep width (Δ) to the MAS rate ($\omega_{rot} = 2\pi\cdot\nu_{rot}$, Section 3.4). As detailed below, BRAIN-CP/WCPMG-MAS offers further advantages with respect to conventional CP, such as reduced power requirements, increased bandwidths for polarization transfer, and high efficiency at slow to moderate MAS rates (10 to 25 kHz).

3.2 FS pulses for spin-locking under MAS

Crucial to the success of any direct-detection CP experiment is the ability to efficiently spin lock the *S* magnetization produced from the *I* source magnetization. Pell and coworkers have demonstrated the ability to efficiently spin lock *S* magnetization across UW frequency ranges using S^{3}APs in inversion experiments.[28] Importantly, these experiments were limited to inversion of spin polarization and did not involve cross-polarization. Early stages of the work with S^{3}APs were limited to the "low-power" regime, delineated by the condition $|\omega_{1,S}| \ll |\omega_{rot}|$,[25] wherein the pulse irradiates only one SSB and thus avoids interference effects from its neighboring sidebands. However, later findings suggest this low power condition is not a strict requirement, especially in applications to UW SSB manifolds where values of $|\omega_{1,S}| \approx |\omega_{rot}|$ also result in efficient inversion.[28]

Previous experiments involving the use of S^{3}APs for inversion ensured that Ω_S was set such that the frequency sweep traversed the resonance frequency of the SSB of highest intensity.[25] In the low-power limit, this ensures inversion of

the highest efficiency due to the fact that the most intense SSB represents a frequency at which resonance between most isochromats and the pulse is achieved at some point throughout the rotor period. Yet, efficient inversion has been reported with Ω_S set to irradiate other SSBs of lower signal intensities, suggesting this condition need not be strictly met.[27] Furthermore, complete inversion of all isochromats is not a rigid requirement for acquisition of a SSB manifold that allows for extraction of the corresponding CS tensor.

The ability to achieve efficient spin locking at multiple combinations of $\omega_{1,S}$ and Ω_S provides experimental flexibility, yet also raises questions concerning which (if any) of these combinations are superior. Numerical simulations (Fig. S2) demonstrate that the choice of the transmitter offset ($\Omega_S/2\pi$) can be correlated with the inversion efficiency, especially with the use of spin locking powers exceeding the MAS rate.

The correlation between the optimal value of $\Omega_S/2\pi$ and inversion efficiency can be rationalized through an analysis of the Hamiltonian describing the S^{3}AP in the jolting frame (J-frame). First introduced by Caravatti and coworkers,[43] the J-frame is one that rotates synchronously with the time dependent chemical shift frequency for a single isochromat and is necessarily orientation dependent. Generally, FS pulses are described in the frequency modulated (FM) frame,[44] which is one wherein the time dependence of the phase arises in the form of a linear frequency sweep. Accordingly, a description of the transformations from the FM frame to the J-frame to the MAS frame is presented in S2. The final frame represents one wherein the time dependence of the CS has been transferred to the RF pulse amplitude term with the effective frequency given by:

$$\omega_{e,S}^{J,rot}(\beta,t,m)=\sum_{m=-\infty}^{+\infty}\left[\left(\Omega_S-m\omega_{rot}-\omega_p(t)\right)^2+\left(\omega_{1,S}A(t)B_m(\beta)\right)^2\right]^{1/2} \quad (1)$$

where Ω_S is the transmitter offset in the rotating frame, ω_{rot} is the MAS rate, $\omega_p(t)$ = d$\varphi(t)$/dt is the instantaneous (*i.e.*, time-dependent) transmitter frequency arising from the phase modulation, $\varphi(t)=\pm2\pi\{(\Delta/2)t-(\Delta/2\tau_{CT})t^2\}$, and $A(t)=1-|\cos(\pi t/\tau_{CT})|^N$ is the amplitude modulation (here N is an integer, commonly set to 2, 20, or 80; herein, values of 2 or 20 are used), and τ_{CT} is the contact pulse length. The terms $\sum_{m=-\infty}^{=\infty}B_m(\beta)=1$ are the Fourier coefficients of the mth SSB in the J-frame wherein $\omega_{e,S}^{J,rot}(\beta, t, m)$ is simultaneously swept across each mth SSB with an amplitude $\omega_{1,S}$ scaled by the factor $B_m(\beta)$ (see eqn (S12) for definition). Each component of $\omega_{e,S}^{J,rot}(\beta, t, m)$ can be evaluated in the J-frame in terms of its effective offset, $\Omega_S^e(t, m) = \Omega_S - m\omega_{rot} - \omega_p(t)$, and effective amplitude, $\omega_{1,S}^e(t, m) = \omega_{1,S}A(t)B_m$. In the event that $\Omega_S^e(t, m) \gg \omega_{1,S}^e(t, m)$ at all times throughout the duration of the pulse, the $\omega_{1,S}^e(t, m)$ terms can be ignored, allowing for an approximation of eqn (1) as:

$$\omega_{e,S}^{J,rot}(t,m)\approx\sum_{m=-\infty}^{+\infty}\Omega_S-m\omega_{rot}-\omega_p(t) \quad (2)$$

The ratio of $\Omega_S^e(t, m)$ and $\omega_{1,S}^e(t, m)$ (and thus the validity of eqn (2) in approximating the effective frequency) can be controlled through several combinations of experimental settings. In general, low-intensity SSB correspond to small values of B_m, thereby allowing for the corresponding $\omega_{1,S}^e(t, m)$ terms to be safely neglected. Such situations arise naturally in applications to UW SSB manifolds (wherein $B_m \ll 1$), but can also be induced through the use of higher magnetic fields and/or the use of slower MAS rates. The use of lower amplitudes $\omega_{1,S}$ also serve to validate the use of eqn (2), but this runs the risk of diminishing spin locking efficiency, especially at slow MAS rates. Furthermore, the validity of eqn (2) can be controlled by an appropriate selection of the experimental value of Ω_S. Tuning Ω_S adjacent to SSBs of high signal intensity generally serves to decrease the ratio $\Omega_S^e(t, m)$: $\omega_{1,S}^e(t, m)$ for the components of $\omega_{e,S}^{J,rot}(\beta, t, m)$ at those SSBs. Alternatively, tuning Ω_S to SSBs of lower intensity results in increased ratios $\Omega_S^e(t, m)$: $\omega_{1,S}^e(t, m)$ for all components $\omega_{e,S}^{J,rot}(\beta, t, m)$ and thus supports the use of eqn (2) in approximating their effective frequencies. Evidence for such a claim can be found in the offset dependent inversion behavior observed in numerical simulations (Fig. S2).

The theoretical insight gained from investigation into pulse parameters enabling efficient spin-locking with S^{3}APs is used to guide choices for optimizing the BRAIN-CP/WCPMG-MAS experiment. In all cases, the condition

$$2\pi\Delta = \omega_{1,S} = \omega_{rot} \quad (3)$$

is fulfilled. In general, the optimal value of Ω_S is determined through experimental optimizations. Pre-existing knowledge of the axial symmetry parameter describing the CS tensor of the target nucleus can be helpful for a starting point for setting Ω_S. However, such insight is not a strict requirement given that signal is obtained if Ω_S is tuned adjacent to any of the SSBs (*vide infra*), albeit giving rise to distorted SSB manifolds in some cases. Notably, numerical simulations suggest that the offset dependency is reduced at faster MAS rates (Fig. S4).

3.3 FS pulses for broadband CP under MAS

Optimal fulfillment of the HH matching conditions ensures maximum polarization transfer efficiency in any CP experiment. The HH matching conditions for CP/MAS experiments employing standard rectangular pulses (*i.e.*, no amplitude or phase modulations) are well understood.[45–47] Due to sample rotation, the dipolar frequency takes on a time dependence and can be expressed as $\omega_D^{IS}(t) = \sum_{m=-2}^{+2} b_m e^{im\omega_{rot}t}$, where b_m are the Fourier coefficients. Provided $\omega_{rot} > |b_m|$, a time dependence is imparted upon the HH matching conditions, which can be expressed in a frame rotating synchronously with the rotor as[45,48]

$$\omega_{e,I} \pm \omega_{e,S} = \pm n\cdot\omega_{rot} \quad (4)$$

where $\omega_{e,I}$ is usually approximated as $\omega_{1,I}$ and $\omega_{e,S} \approx (\Omega_S^2 + \omega_{1,S}^2)^{1/2}$, and n is usually 1 or 2. The sum and difference of the frequencies in eqn (4) are commonly referred to as the double-quantum (DQ) and zero-quantum (ZQ) matching conditions, respectively.

Use of a S^{3}AP introduces a time dependence to eqn (4):

$$\omega_{1,I} \pm \omega_{e,S}(t) = \pm n \cdot \omega_{rot} \quad (5)$$

where

$$\omega_{e,S}(t) = [(\Omega_S - \omega_p(t))^2 + (\omega_{1,S}A(t))^2]^{1/2}. \quad (6)$$

3.3.1 HH matching: time-independent chemical shift. Numerical simulations (Fig. 2) are used to verify to the time dependent matching conditions as predicted by eqn (5). The spin system consists of a pair of spin-1/2 nuclides (I = ^{1}H, S = ^{13}C) with a coupling described by $b_D^{IS}/2\pi$ = 4 kHz. The ^{1}H spin is assumed to have no CSA whereas that of the ^{13}C spin is described by δ_{iso} = 0 ppm, Ω_{CS} = 1350 ppm, and κ = −1 using the Herzfeld-Berger convention. From a starting density matrix of $\rho(t = 0) = \langle \mathbf{I}_x \rangle$, the expectation value $\langle \mathbf{S}_z \rangle$ is calculated immediately following the application of simultaneous spin locking pulse applied to each spin for a duration τ_{CT} = 10 ms. A rectangular pulse with an amplitude $\nu_{1,I}$ is applied to the ^{1}H spin on-resonance and a S^{3}AP is applied to the ^{13}C spin with the phase modulation set according to eqn (1) such that $\Delta = \nu_{1,S} = \nu_{rot}$ = 15 kHz. Variation of both $\nu_{1,I}$ and the S^{3}AP offset, $\Omega_S/2\pi$, give rise to the matching conditions represented in the contour plot shown in Fig. 2. Regions of dark red and light yellow are indicative of efficient CP, resulting in both negative and positive values of $\langle \mathbf{S}_z \rangle$, respectively.

A wide range of matching conditions, as determined by various combinations of offsets and amplitudes, are available in BRAIN-CP/MAS experiments and the selected conditions influence the resulting sign of $\langle \mathbf{S}_z \rangle$ upon conclusion of the contact pulse (NB: distinction is made between BRAIN-CP/MAS, referring only to the CP period, and BRAIN-CP/WCPMG-MAS, referring to the experimental combination of BRAIN-CP with WCPMG-MAS). The effective offset, $\Omega_{S,e}(t) = \Omega_S - \omega_p(t)$, is defined from eqn (6) and its instantaneous sign dictates that of $\langle \mathbf{S}_z \rangle$. The impact of the sign of $\Omega_{S,e}(t)/2\pi$ is evaluated through inspection of the time trajectories of both $\langle \mathbf{I}_x \rangle$ and $\langle \mathbf{S}_z \rangle$ using different values of $\Omega_S/2\pi$ (Fig. 3). In all simulations, the direction of the frequency sweep is from low to high frequency and $\nu_{1,I}$ = 10 kHz. The time trajectories of $\Omega_{S,e}(t)/2\pi$ for two different values of $\Omega_S/2\pi$ are shown relative to the resonance frequency of the S spin (Fig. 3a). The two cases for consideration are $\Omega_S/2\pi$ = +5 kHz (Fig. 3b and c) and +10 kHz (Fig. 3d and e). Solutions to eqn (5) (Fig. 3b and d) predict the fulfillment of DQ matching conditions at times close to the start of the FS for both cases. Indeed, the simultaneous buildups of $\langle \mathbf{S}_z \rangle$ and decreases in $\langle \mathbf{I}_x \rangle$ agree with this prediction (Fig. 3c and e). The opposite signs of $\langle \mathbf{S}_z \rangle$ towards the start of the contact pulse in Fig. 3c and e are attributed to the signs of $\Omega_{S,e}(t)/2\pi$ relative to the resonance frequency of the target spin isochromat during the time at which the matching conditions are met: an offset of $\Omega_S/2\pi$ = +5 kHz makes $\Omega_{S,e}(t)/2\pi$ negative at this point, whereas for $\Omega_S/2\pi$ = +10 kHz, $\Omega_{S,e}(t)/2\pi$ is positive at all times (Fig. 3a). In the case of $\Omega_S/2\pi$ = +5 kHz (Fig. 3c), the resonance condition is traversed shortly after the matching condition is met, which results in the inversion of $\mathbf{S}_z$ (*i.e.*, $\langle \mathbf{S}_z \rangle < 0$). Inversion is not observed in the case of $\Omega_S/2\pi$ = +10 kHz (Fig. 3d and e) as the resonance condition is avoided. The fulfillment of additional matching conditions in the latter case explains the observed oscillatory transfer between the I and S spin polarization. Changing the sign of Ω_S to a negative value results in $\langle \mathbf{S}_z \rangle$ with signs opposite to those discussed above, as does reversing the direction of the frequency sweep from high to low frequency (Scheme S3). Thus, it is a combination of factors that affect the sign of $\langle \mathbf{S}_z \rangle$ produced in the BRAIN-CP/MAS experiment: the sign of Ω_S, the sign of $\Omega_{S,e}(t)$ at the point in time in which the match is fulfilled, the direction of the frequency sweep, and whether or not the sweep traverses the resonance condition. Additionally, the nature of the matching condition (*i.e.*, either ZQ or DQ) influences the sign of $\langle \mathbf{S}_z \rangle$ produced in BRAIN-CP/MAS experiments (Fig. S5).

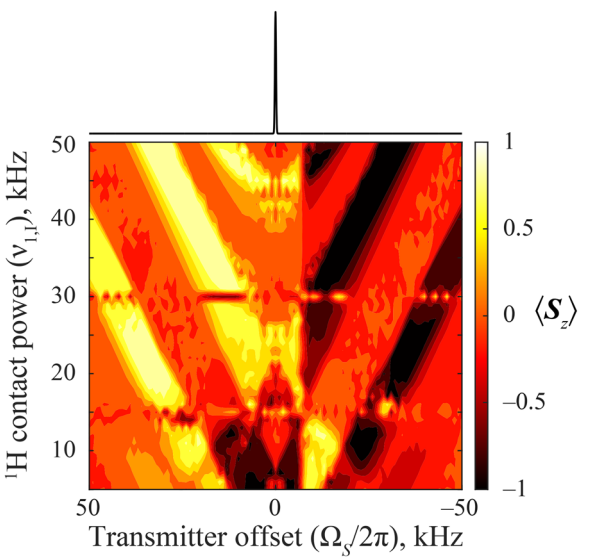

Fig. 2 Numerical simulations of BRAIN-CP/MAS $I \rightarrow S$ polarization transfer for a two-spin system (I = ^{1}H, S = ^{13}C) under MAS conditions of ν_{rot} = 15 kHz. The ^{13}C chemical shift tensor parameters are: δ_{iso} = 0 ppm, Ω_{CS} = 1350 ppm, and κ = −1. The β = 0° isochromat is used, where β is the angle between σ_{zz} and the rotor axis. The ideal single crystal spectrum is shown above the contour plot. The expectation value $\langle \mathbf{S}_z \rangle$ is plotted as a function of $\nu_{1,I}$ and $\Omega_S/2\pi$ for simulations wherein $\Delta = \nu_{1,S} = \nu_{rot}$ = 15 kHz. The contact time τ_{CT} is 10 ms and the heteronuclear dipolar coupling is given by $b_D^{IS}/2\pi$ = 4 kHz with the dipolar vector oriented at θ = 45° relative to the rotor.

Similarities between conventional CP/MAS and BRAIN-CP/MAS are observed, despite the time dependence of the HH matching conditions in the latter which can convolute such comparisons. The sign of the magnetization produced in both experiments depends on both the sign of the effective frequencies on both channels fulfilling the matching condition and the nature of the matching condition.[49] In principle, a plot demonstrating the HH matching conditions for CP/MAS experiments in a manner similar to that of BRAIN-CP/MAS experiments (Fig. 2) could be envisioned. However, there exist no previous studies showcasing such results. This is largely due to the fact that CP/MAS experiments targeting spin-1/2 nuclides typically employ RF pulses with amplitudes on the order of 50 kHz to

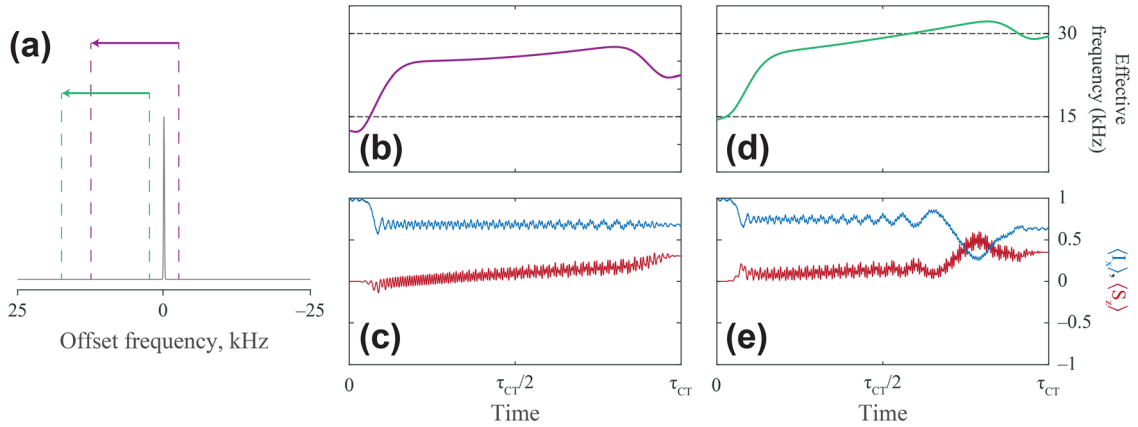

Fig. 3 (a) Ideal simulation for the isochromat oriented at $\beta = 0^\circ$ with respect to the rotor axis. Purple and green arrows indicate the frequency ranges traversed by S^3AP's centered at $\Omega_S/2\pi$ = 5 kHz and 10 kHz, respectively. Analytical (b) and (d) and numerical (c) and (e) simulations for BRAIN-CP/MAS $I \rightarrow S$ polarization transfer during a S^3AP under MAS conditions of ν_{rot} = 15 kHz using $\Omega_S/2\pi$ = 5 kHz (b) and (c) and 10 kHz (d) and (e). Analytical plots show DQ solutions to eqn (5) of the main text. Numerical simulations make use of a two-spin system ($I = {}^1$H, $S = {}^{13}$C) with the ^{13}C chemical shift tensor parameters described by: δ_{iso} = 0 ppm, Ω_{CS} = 1350 ppm, and $\kappa = -1$. In all cases, $\nu_{1,I}$ = 10 kHz and $\Delta = \nu_{1,S} = \nu_{rot}$ = 15 kHz. The contact time τ_{CT} is 10 ms and the heteronuclear dipolar coupling is given by $b_D^{IS}/2\pi$ = 4 kHz with the dipolar vector oriented at $\theta = 45^\circ$ relative to the rotor.

ensure efficient spin-locking. The potential for fulfilling as many matching conditions as are depicted in Fig. 2 only arise with the unique combination of low power RF pulses and slow MAS rates. Such experimental protocols have the distinct effect of clustering the matching conditions together in small frequency ranges relative to those at faster MAS rates and/or those with the use of higher powers. Thus, while the spin physics governing the polarization transfers in both CP/MAS and BRAIN-CP/MAS experiments are similar, it is the ability to efficiently spin-lock S magnetization at low RF powers using S^3APs that differentiates the two experiments and offers the potential for a wide range of accessible matching conditions in the BRAIN-CP/MAS experiment.

3.3.2 HH matching: time-dependent chemical shift. Consideration of an isochromat with a time-dependent chemical shift is more representative of the spin dynamics occurring within a powder sample, yet involves considerably more complex spin behavior. However, use of the J-frame allows for an approximation of the HH matching conditions as:

$$\omega_{1,I} = \omega_{e,S}^{J,rot}(\beta, t, m) \pm n\cdot\omega_{rot} \quad (7)$$

where $\omega_{e,S}^{J,rot}(\beta, t, m)$ is given in eqn (1). Comparison between numerical simulations for BRAIN-CP/MAS transfer conducted in the FM- and J-frames are indistinguishable, suggesting that both represent equivalent ways to describe the spin dynamics (Fig. S6, S7 and Table S3). As detailed above, the J-frame represents one wherein the effective frequency sweep occurs simultaneously across each SSB. In the limit of large CSA's, the impact of $\omega_{1,S}$ on the frequency sweep in the J-frame is negligible, as can be appreciated from eqn (2). Thus, the HH matching conditions can be inspected by evaluating solutions to eqn (7) corresponding to different m-components of $\omega_{e,S}^{J,rot}(\beta, t, m)$.

Differing only by the orientation of the S spin isochromat as determined by the angle β, a spin system otherwise identical to the one described above for I–S BRAIN-CP/MAS transfer (Fig. 2 and Fig. S5) is used to demonstrate the influence of a time-dependent chemical shift on the HH matching conditions. The isochromat described by $\beta = 35^\circ$ is chosen and simulated values of $\langle \mathbf{S}_z \rangle$ are used to create a contour plot (Fig. 4) that enables visualization of the HH matching conditions as a function of $\nu_{1,I}$ and $\Omega_S/2\pi$, as was done similarly in Fig. 2. This time, the observed matching conditions follow a strikingly different pattern. Narrow bands of light yellow and dark red, again indicating efficient polarization to produce high values of $\langle \mathbf{S}_z \rangle$ in the positive and negative directions, respectively, are centered around each SSB.

A J-frame analysis can be used to rationalize the HH matching conditions for the case of the time-dependent chemical shift, as verified by a comparison of the analytical and

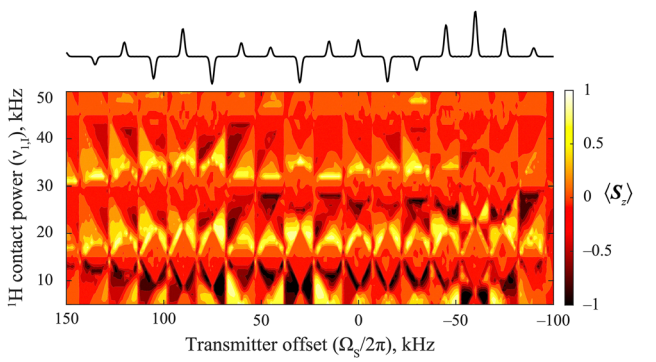

Fig. 4 Numerical simulations of BRAIN-CP/MAS $I \rightarrow S$ polarization transfer for a two-spin system ($I = {}^1$H, $S = {}^{13}$C) under MAS conditions of ν_{rot} = 15 kHz. The ^{13}C chemical shift tensor parameters are: δ_{iso} = 0 ppm, Ω_{CS} = 1350 ppm, and $\kappa = -1$. The $\beta = 35^\circ$ isochromat is used, where β is the angle between σ_{zz} and the rotor axis. The ideal single crystal spectrum is shown above the contour plot. The expectation value $\langle \mathbf{S}_z \rangle$ is plotted as a function of $\nu_{1,I}$ and $\Omega_S/2\pi$ for simulations wherein $\Delta = \nu_{1,S} = \nu_{rot}$ = 15 kHz. The contact time τ_{CT} is 10 ms and the heteronuclear dipolar coupling is given by $b_D^{IS}/2\pi$ = 4 kHz with the dipolar vector oriented at $\theta = 45^\circ$ relative to the rotor.

numerical simulations (Fig. S8). As in the case of the isotropic chemical shift, the sign of $\langle \mathbf{S}_z \rangle$ at $t = \tau_{CT}$ hinges upon several factors, including the direction of the FS, the nature of the matching condition, and the relative time occurrences of the matching condition and the traversal of the resonance condition. Interestingly, the J-frame analysis results in a description of several matching conditions met simultaneously as a result of the consideration of each individual component of $\omega_{e,S}^{J,rot}(\beta, t, m)/2\pi$ (Fig. S8).

3.3.3 HH matching: powder averaging. Results similar to those observed for the case of a time-dependent chemical shift are evident in the powder-averaged matching conditions (Fig. 5). Provided $\Omega_S/2\pi$ is tuned adjacent to any SSB, matching conditions are observed in bands centered around each SSB. A slight drop in efficiency is observed at negative frequency offsets, particularly around the SSBs of highest signal intensity. The validity of the J-frame approximation (and thus that of eqn (7)) is lowest for these latter SSBs, suggesting that complete neglect of the value of $\nu_{1,S}$ may not be appropriate. Indeed, the possibility for fulfillment of matching conditions resulting in destructive interference of S magnetization arises – behavior that is enhanced with smaller CSAs (Fig. S9), for which the J-frame approximation breaks down further.

3.3.4 HH matching: experimental validation. Experimental tests of the predicted matching conditions were conducted by acquiring ^{1}H–^{119}Sn BRAIN-CP/WCPMG-MAS spectra of [Sn(HPDABA)]Cl_2 at three different optimized values of $\Omega_S/2\pi$ (between SSBs near the center of gravity, as well as between SSBs at the low and high frequency edges of the SSB manifold, Fig. 6). In all cases, $\nu_{1,I}$ is arrayed from 10 to 50 kHz in increments of 1 kHz with τ_{CT} = 10 ms and $\Delta = \nu_{1,S} = \nu_{rot}$ = 15 kHz, the condition represented by eqn (3) and is supported by experimental evidence in BRAIN-CP/WCPMG-MAS experiments (Fig. S11). In all three cases, signal is obtained between both the ^{1}H rotary resonance conditions appearing at intervals of $\nu_{1,I} = n\nu_{rot}$[50] and the null points appearing at half-integer multiples of ν_{rot}. Discrimination between ZQ and DQ matching conditions is obscured due to the fact that all spectra are processed in magnitude mode. As predicted by analytical and numerical simulations (*vide supra*), all values of $\Omega_S/2\pi$ except those both resonant with and halfway between SSBs are successful at producing some signal. However, the performance is markedly better with $\Omega_S/2\pi$ tuned near the low-frequency (right) end of the CSA pattern. As detailed in Section 3.2, this is due to the relationship between spin locking efficiency and the degree of axial symmetry of the S-spin CS tensor.

Qualitative agreement between experimental and theoretical data is observed, yet several discrepancies exist. The most apparent difference is the dependence of the observed matching conditions on the parameters $\Omega_S/2\pi$ and $\nu_{1,I}$ (Fig. S10). While simulations predict narrow-banded matching conditions (Fig. 5), experimental data suggests a broadening of these conditions (Fig. S11), with maximal signal obtained when $\Omega_S/2\pi$ is between two consecutive SSBs and $\nu_{1,I}$ takes on a value between half-integer multiples of ν_{rot}. Several factors could contribute to such behavior, including the inability to perfectly model spin dynamics using a two-spin system (see Fig. S12), broadening of the matching conditions due to the range of homonuclear dipolar couplings present in solids, and/or RF inhomogeneity. However, both theory and experiment similarly predict null signal obtained using $\nu_{1,I}$ of half-integer multiples of ν_{rot}. In contrast to simulations which predict maximal CP efficiency using values of $\nu_{1,I}$ closer to ν_{rot}, experimentally it is maximized at higher values of $\nu_{1,I}$. This is attributed to inefficient spin locking on the I channel using low RF pulse powers (*i.e.*, short $T_{1\rho}(^{1}H)$, see Fig. S13). Drawing upon the results presented in this section, a recommended starting value of $\nu_{1,I}$ is one halfway between the half-integer multiples of ν_{rot}. At slow MAS rates, higher powers are recommended to ensure efficient spin-locking.

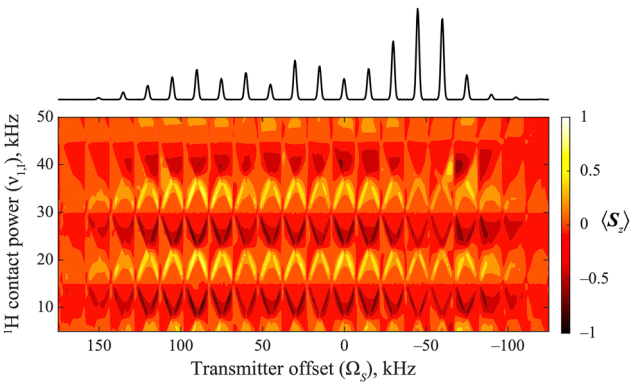

Fig. 5 Numerical simulations of BRAIN-CP/MAS $I \rightarrow S$ polarization transfer for a two-spin system (I = ^{1}H, S = ^{13}C). The ^{13}C chemical shift tensor parameters are: δ_{iso} = 0 ppm, Ω_{CS} = 1350 ppm, and $\kappa = -1$. The expectation value $\langle \mathbf{S}_z \rangle$ is plotted as a function of $\nu_{1,I}$ and $\Omega_S/2\pi$ and powder averaged with the REPULSION scheme. Maximum signal is indicated by the yellow (positive) and dark red (negative) regions. The ideal MAS SSB manifold is shown above the contour plot. In all cases, $\nu_{1,S} = \Delta = \nu_{rot}$ = 15 kHz. The contact time τ_{CT} is 10 ms and the heteronuclear dipolar coupling is given by $b_D^{IS}/2\pi$ = 4 kHz with the dipolar vector oriented at $\theta = 45°$ relative to the rotor.

3.4 On the choice of MAS rate and contact time

The choice of MAS rate for BRAIN-CP/WCPMG-MAS experiments is somewhat arbitrary and ultimately left to the experimentalist. In general, $\nu_{rot} > 10$ kHz seems to be advantageous in terms of maximizing SNR, but, as with most choices in NMR, there are pros and cons associated with the specific choice of ν_{rot}. The optimal value for ν_{rot} ultimately depends on the attainable spin locking amplitudes (due to the requirement that $\nu_{1,S} = \nu_{rot}$) and width of the SSB manifold (due to the direct relationship between $\nu_{exc/ref}$ and $\nu_{rot}{\cdot}\Omega_{CS}$, see Section 3.2). The use of very slow MAS rates is likely not optimal as spin-locking efficiency is expected to suffer. Simulations and experiments similar to those presented in Fig. 5 and 6 were carried out at a ν_{rot} = 10 kHz (Fig. S14 and S15), with results similar to those discussed above. While uniform experimental SSB manifolds are produced at different values of ν_{rot}, faster MAS rates generally result in higher SNRs. This can be attributed to two factors: (i) higher MAS rates tend to give increased SNRs due to localization of signal in fewer SSBs; and (ii) the dependence of

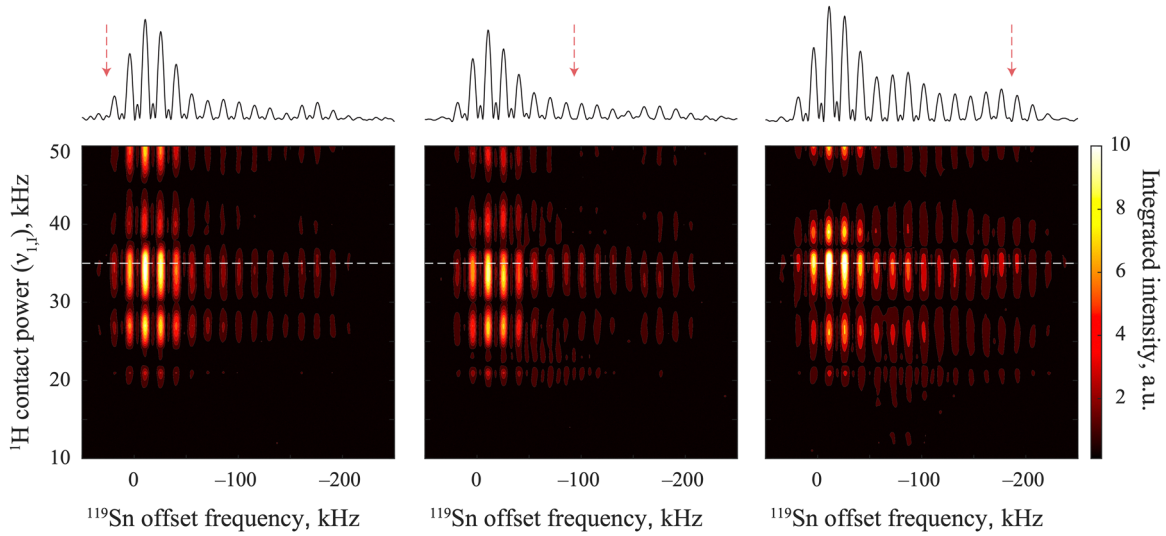

Fig. 6 Contour plot showing ^{1}H–^{119}Sn BRAIN-CP/WCPMG-MAS NMR spectra of [Sn(HPDABA)]Cl_2 acquired at 14.1 T as a function of ^{1}H contact power, $\nu_{1,I}$, using three different offsets $\Omega_S/2\pi$, as indicated by the red arrows above each spectrum. For all experiments, $\nu_{1,S} = \Delta = \nu_{rot}$ = 15 kHz, and τ_{CT} = 10 ms. The spectra displayed above each contour plot are acquired with $\nu_{1,I}$ = 34 kHz.

the HH match on ν_{rot} is such that faster MAS rates demand higher values for $\nu_{1,I}$, which in turn results in better ^{1}H spin locking. This latter point comes with several caveats: (i) high-powered pulses on both channels place more demand on the NMR probe, especially for experiments on low-γ nuclides; (ii) larger values of ν_{rot} decrease the number of SSBs, which can cause an increased dependence of the BRAIN-CP/MAS experiment on $\Omega_S/2\pi$; (iii) faster MAS rates also require increased rates $R_{exc/ref}$ for the WCPMG excitation and refocusing pulses, in order to obtain high values of x,[14] which in turn require higher amplitudes;[51] and (iv) very fast MAS rates are known to reduce CP efficiency and would thus introduce further complications to the experiment.[52,53]

Directly dependent on the MAS rate is the spacing of rotary echoes in each CPMG loop. As mentioned in Section 3.1, the echo length, τ_{SE}, and thus, the number of rotary echoes acquired, influence the appearance of the NMR spectra, with shorter echo lengths resulting in spectral distortions present in many of the spectra shown herein. However, shorter values of τ_{SE} allow for the acquisition of more CPMG echoes and thus result in spectra with higher SNRs, albeit with decreased resolution (this poses no issues if only one site is expected). We note that these distortions do not hinder the extraction of CS tensor parameters and thus, the choice of τ_{SE} is left to the experimentalist.

A final comment is directed towards the choice of the contact time, τ_{CT}. As with conventional CP (both static and MAS) and static BRAIN-CP experiments, intuition concerning the relative magnitudes of the heteronuclear couplings can help determine initial values for τ_{CT}. However, the optimal value of τ_{CT} is generally deciphered through experimental optimizations (Fig. S16). Values of τ_{CT} below several milliseconds are not advised, as these are unlikely to allow for sufficient polarization transfer and run the additional risk of decreasing the spin locking efficiency.

4. Experimental examples

Having established the theoretical principles governing the spin dynamics in the BRAIN-CP/WCPMG-MAS, several test cases are presented that demonstrate its capability, versatility, and robustness. First, a case of a non-axially symmetric ^{119}Sn CS tensor is investigated. Then, a ^{195}Pt example is chosen to showcase the ability to CP across bandwidths approaching 1 MHz. Finally, an example of ^{103}Rh SSNMR is shown as a demonstration of the acquisition of wideline SSNMR SSB manifolds of low-γ nuclides.

4.1 Wideline ^{1}H–^{119}Sn BRAIN-CP/MAS NMR: a case of a non-axially symmetric CS tensor

Thus far, all theoretical and experimental examples have focused on *S* nuclides with axially symmetric CS tensors; hence, the case of DBTO is presented to demonstrate that the principles outlined above also apply to systems in which the CS tensor is not axially symmetric. Excellent agreement is observed between the ideal and experimental ^{119}Sn SSB manifolds of DBTO acquired at 14.1 T and with ν_{rot} = 12 kHz (Fig. 7). As in the case of axially symmetric CS tensors, values of $\Omega_S/2\pi$ that position the transmitter near the edge of the SSB manifold provide more efficient spin locking and thus result in more efficient CP (see again Fig. S4). The experimentally optimized matching conditions are $\nu_{1,S}$ = 12 kHz and $\nu_{1,I}$ = 40 kHz. Predictions for the optimal HH matching conditions for $\nu_{1,I}$ falling between both odd and even half-integer multiples of ν_{rot} include $\nu_{1,I} \approx$ 15, 21, 27, or 43 kHz, for which the optimized value of $\nu_{1,I}$ = 40 kHz is close.

Similar to the case of [Sn(HPDABA)]Cl_2, the $T_1(^{119}Sn)$ is several orders of magnitude larger than the $T_1(^1H)$ and thus, ^{1}H–^{119}Sn BRAIN-CP/WCPMG-MAS experiments represent a much more efficient method of acquisition relative to DE methods.[54] While spectral acquisition *via* BRAIN-CP/WCPMG-MAS was

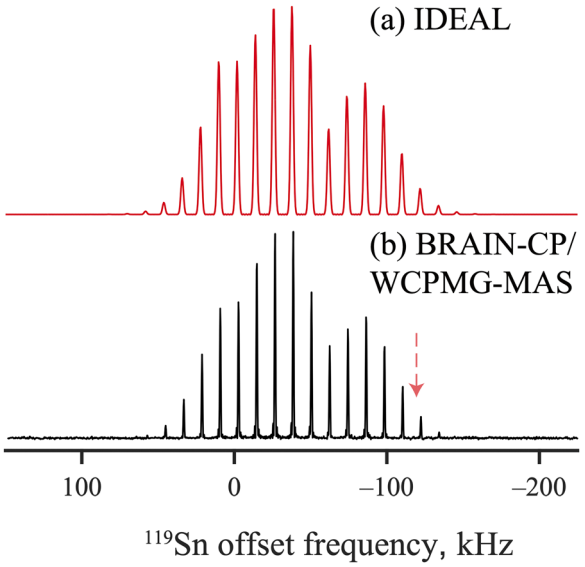

Fig. 7 (a) Simulated and (b) experimental ^{119}Sn MAS NMR spectra of DBTO acquired at 14.1 T using BRAIN-CP/WCPMG-MAS with $\nu_{1,S} = \Delta = \nu_{rot}$ = 12 kHz, τ_{CT} = 10 ms, and $\nu_{1,I}$ = 17 kHz. The value of $\Omega_S/2\pi$ is indicated by the dotted red arrow.

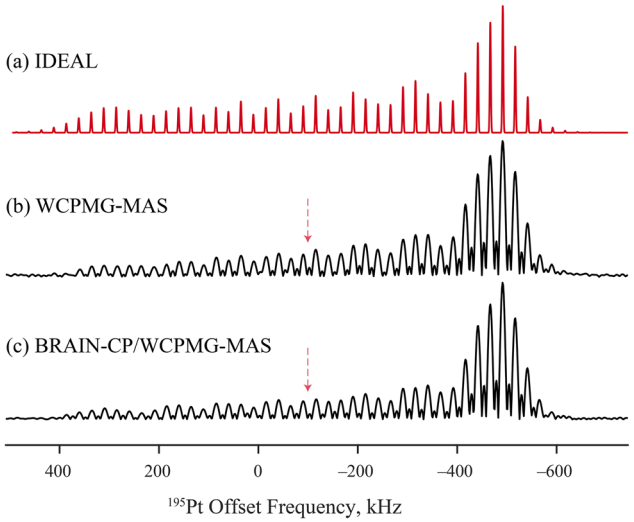

Fig. 8 (a) Simulated and (b) and (c) experimental ^{195}Pt MAS NMR spectra of cisplatin acquired at 11.7 T using (b) WCPMG/MAS and (c) BRAIN-CP/WCPMG-MAS with $\nu_{1,S} = \Delta = \nu_{rot}$ = 25 kHz, τ_{CT} = 10 ms, and $\nu_{1,I}$ = 42 kHz. Experimental values of $\Omega_S/2\pi$ are indicated by the dotted red arrows. 256 transients were collected for both experimental spectra using recycle delays of (b) 60 s and (c) 5 s, for a total time of *ca.* 4.3 hours and 21 minutes, respectively.

accomplished in just 32 seconds (Fig. 7), WCPMG-MAS acquisition with the same number of scans is predicted to take *ca.* 7 hours and was thus not attempted.

4.2 Ultra-wideline ^{1}H–^{195}Pt BRAIN-CP/MAS experiments: pushing the CP bandwidth capability

^{195}Pt is oftentimes selected as a target for methods aimed at the acquisition of wideline and UW NMR powder patterns.[2,55–58] The ^{195}Pt NMR SSB manifold of cisplatin spans 965 kHz (8975 ppm)[59] in breadth at 11.7 T (Fig. 8). Here, the WCPMG-MAS (Fig. 8b) and BRAIN-CP/WCPMG-MAS (Fig. 8c) NMR experiments at MAS rates of ν_{rot} = 25 kHz both enable acquisition of ^{195}Pt NMR spectra displaying the entire SSB manifold at a single transmitter frequency; however, the experimental time required for acquisition of the BRAIN-CP/WCPMG-MAS spectrum (Fig. 8c) is significantly shorter than that of the WCPMG spectrum of similar quality (21 min. compared to 4.3 hours) due to the shorter recycle delay in CP experiments afforded from the shorter $T_1(^1\text{H})$ relative to the $T_1(^{195}\text{Pt})$. Starting with a predicted value of $\nu_{1,I} \approx$ 44 kHz, that obtained from experimental optimizations is $\nu_{1,I}$ = 42 kHz.

The large span of the ^{195}Pt NMR SSB manifold of cisplatin likely serves to reduce the offset dependency of the BRAIN-CP/WCPMG-MAS experiment and thus tuning $\Omega_S/2\pi$ adjacent to any SSB should provide sufficient spin locking. To minimize the RF amplitude required for WURST excitation and refocusing pulses, $\Omega_S/2\pi$ is set close to the center of the SSB manifold. Deviations from this central position would require an increase in the already demanding RF amplitude of ν_{RF} = 87 kHz. Importantly, the amplitude shape modulation parameter N is set to 2, which has been shown to greatly facilitate the excitation and refocusing capability of such pulses in applications to UW SSB manifolds.[14]

4.3 Wideline ^{1}H–^{103}Rh BRAIN-CP MAS experiments: a low-gamma application

^{103}Rh presents a challenging case for acquisition of NMR signal due to its very low gyromagnetic ratio (γ = –0.8486 × 10^7 rad T^{-1} s^{-1}). Accordingly, there are very few examples of ^{103}Rh SSNMR spectra to date.[60–64] $Rh_2Cl_2(COD)_2$ has favorable properties for testing the applicability of BRAIN-CP/WCPMG-MAS for the acquisition of SSB manifolds of low-γ nuclides with small heteronuclear dipolar couplings, including a high wt% of Rh and short $T_1(^1\text{H})$, as estimated from an optimized recycle delay of 2 s. The ^{103}Rh NMR SSB manifold (Fig. 9) is in agreement with the ideal simulated SSB manifold. Experimental acquisition was accomplished in 2.3 hours at ν_{rot} = 14 kHz using experimentally optimized matching conditions of $\nu_{1,S}$ = 14 kHz and $\nu_{1,I}$ = 35 kHz. For the same reasons as those outlined in Section 4.2, the transmitter was tuned near the center of the pattern. As observed in other spectra presented herein, the peaks present between SSBs are a result of the use of short τ_{SE} (see Section 3.4).

5. A summary of guidelines for setting up BRAIN-CP/WCPMG-MAS experiments

Here, we provide a set of guidelines for preliminary setup of the BRAIN-CP/WCPMG-MAS pulse sequence. It is noted that as with conventional CP/MAS experiments, there is some degree of optimization necessary – but the following information provides a good starting point, at the very least.

(i) The choice of MAS rate, ν_{rot}: based on this work, MAS rates between 10 and 25 kHz are recommended. Higher rates

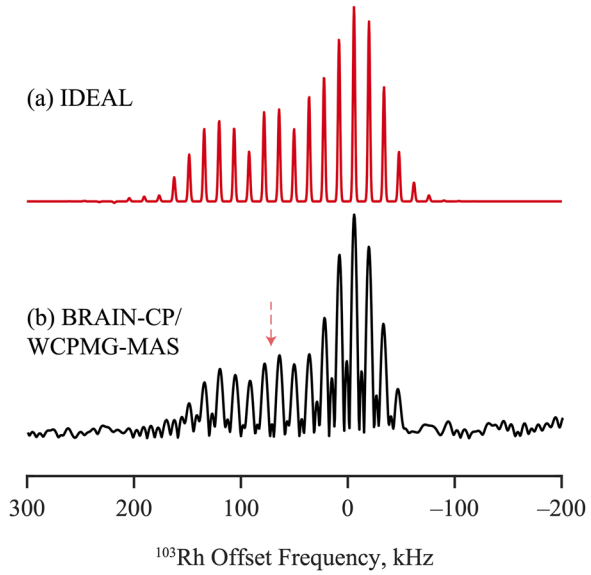

Fig. 9 (a) Simulated and (b) experimental ^{103}Rh MAS NMR spectra of $Rh_2Cl_2(COD)_2$ acquired at 21.08 T using BRAIN-CP/WCPMG-MAS with $\nu_{1,S} = \Delta = \nu_{rot} = 14$ kHz, $\tau_{CT} = 20$ ms, and $\nu_{1,I} = 35$ kHz. The value of $\Omega_S/2\pi$ is indicated by the dotted red arrow. 4096 transients were collected using a recycle delay of 2 s for a total time of *ca.* 2.3 hours.

allow for more efficient ^{1}H spin locking yet also decrease the number of SSBs and thus may introduce an offset dependency. Furthermore, higher MAS rates required higher S RF pulse amplitudes and thus may not be attainable for low-γ nuclei. MAS rates higher than 25 kHz were not explored, but could be the subject of future work.

(ii) Phase and amplitude of S^{3}AP: the condition $2\pi\Delta = \omega_{1,S} = \omega_{rot}$ (eqn (3)) should be fulfilled in order to provide efficient spin locking.

(iii) Contact pulse length, τ_{CT}: pulses on the order of several or tens of milliseconds are optimal. Intuition as to the relative magnitudes of the heteronuclear dipolar couplings can be used for starting points, as is done with conventional CP/MAS experiments.

(iv) Transmitter offset, Ω_S: the exact value of Ω_S should be determined through experimental optimizations, but its optimal values are predicted to normally occur halfway between the half-integer multiples of ν_{rot}. If the symmetry of the CS tensor is known, Ω_S should be tuned adjacent to the SSBs of lower intensities. If δ_{iso} is known, Ω_S can be preliminarily set adjacent to δ_{iso}, in either the positive or negative direction. For UW NMR spectra (*e.g.*, spans in excess of 200 kHz), the choice of tuning to a specific SSB becomes less critical (Fig. 5). Nevertheless, a final optimization of Ω_S in an interval of $-\omega_{rot}/2$ to $+\omega_{rot}/2$ in steps of 1 or 2 kHz around the initially chosen SSB should be conducted in order to optimize CP efficiency.

6. Conclusions

In this work, it is shown how the BRAIN-CP/WCPMG-MAS pulse sequence can be used to acquire wideline and UW spectra of spin-1/2 nuclides featuring SSB manifolds arising from CSA, under conditions of moderate MAS rates (10–25 kHz) and with S contact pulses with low RF amplitudes. Provided the condition $\nu_{rot} = \nu_{1,S} = \Delta$ is met, both DQ and ZQ HH matching conditions can be satisfied when Ω_S is set adjacent to any of the SSBs of the target NMR SSB manifold and $\nu_{1,I}$ is within a few kHz of a half-integer multiple of $\nu_{rot}/2$. Without knowledge of the exact resonance frequency of a SSB, experimental optimizations of Ω_S and $\nu_{1,I}$ are generally required. However, an intuition (*i.e.*, from direct crystallographic information regarding the site symmetry and/or DFT calculations) about the axial symmetry of the CS tensor of the S nucleus can aid in the optimization of Ω_S. The examples of applications of the BRAIN-CP/WCPMG-MAS sequence discussed herein feature nuclides with different gyromagnetic ratios and CS tensors of varying magnitude and symmetry, serving to demonstrate the robustness of this method. We hope that BRAIN-CP/WCPMG-MAS can aid in the routine acquisition of NMR spectra of spin-1/2 nuclides and certain quadrupolar nuclides (with small quadrupolar interactions) having anisotropically broadened patterns arising from CSA and possibly even Knight shift anisotropy. Furthermore, this robust method may even be useful in DNP experiments for the enhancement of wideline and UW NMR spectra, *e.g.*, Pt catalytic centers on surfaces or a wide range of heterogeneous catalysts.

Conflicts of interest

The authors declare that they have no known competing financial interests or personal relationships that could have appeared to influence the work reported in this paper.

Data availability

Pulse sequences used for collection of all data used for main text figures are available at https://github.com/rschurko. Representative setup files sufficient to reproduce the simulation results are provided in the supplementary information (SI). Supplementary information contains description of [Sn(HPDABA)]Cl_2 co-crystal synthesis, additional pulse program schemes. Experimental parameters for all acquired BRAIN-CP/WCPMG-MAS and WCPMG-MAS spectra, analytic derivation of effective S nuclei nutation frequency in the jolting frame, supplementary figures (simulations and experiments), BRAIN-CP/WCPMG-MAS pulse sequence for SIMPSON simulations. See DOI: https://doi.org/10.1039/d5cp03931b.

Acknowledgements

J. J. K. and R. W. S. would like to thank the Basic Energy Sciences Program in the Department of Energy (DE-SC0022310) for supporting this work. Early stages of these projects were supported by the National Science Foundation Chemical Measurement and Imaging Program, with partial co-funding from the Solid State and Materials Chemistry Program (NSF-2003854). Some NMR spectra were acquired at the National

High Magnetic Field Laboratory, which is supported by the National Science Foundation (NSF/DMR-1644779, NSF/DMR-2128556) and the State of Florida. Some of the probe technologies used in this study were developed *via* resources provided by the National Resource for Advanced NMR Technology, an NIH RM1 center (RM1 GM148766). This study made use of NMRbox: National Center for Biomolecular NMR Data Processing and Analysis, a Biomedical Technology Research Resource (BTRR), which is supported by NIH grant P41GM111135 (NIGMS). J. J. K. and R. W. S. are grateful to Dr Zhehong Gan (NHMFL) for helpful discussions on spin dynamics. Jazmine Sanchez is thanked for synthesis of [Sn(HPDABA)]Cl_2.

References

1 R. W. Schurko, *Acc. Chem. Res.*, 2013, **46**, 1985.
2 T. Kobayashi, F. A. Perras, T. W. Goh, T. L. Metz, W. Huang and M. Pruski, *J. Phys. Chem. Lett.*, 2016, **7**, 2322.
3 A. Venkatesh, M. P. Hanrahan and A. J. Rossini, *Solid State Nucl. Magn. Reson.*, 2017, **84**, 171.
4 A. J. Rossini, M. P. Hanrahan and M. Thuo, *Phys. Chem. Chem. Phys.*, 2016, **18**, 25284.
5 L. A. O'Dell and R. W. Schurko, *Chem. Phys. Lett.*, 2008, **464**, 97.
6 A. Tannús and M. Garwood, *NMR Biomed.*, 1997, **10**, 423.
7 M. Garwood and L. DelaBarre, *J. Magn. Reson.*, 2001, **153**, 155.
8 J. M. Bohlen, M. Rey and G. Bodenhausen, *J. Magn. Reson.*, 1989, **84**, 191.
9 J. M. Böhlen, I. Burghardt, M. Rey and G. Bodenhausen, *J. Magn. Reson.*, 1990, **90**, 183.
10 V. L. Ermakov, J. M. Böhlen and G. Bodenhausen, *J. Magn. Reson., Ser. A*, 1993, **103**, 226.
11 Ē. Kupče and R. Freeman, *J. Magn. Reson., Ser. A*, 1995, **115**, 273.
12 L. A. O'Dell, *Solid State Nucl. Magn. Reson.*, 2013, **55–56**, 28.
13 A. W. MacGregor, L. A. O'Dell and R. W. Schurko, *J. Magn. Reson.*, 2011, **208**, 103.
14 J. Koppe, M. Bußkamp and M. R. Hansen, *J. Phys. Chem. A*, 2021, **125**, 5643.
15 S. L. Veinberg, A. W. Lindquist, M. J. Jaroszewicz and R. W. Schurko, *Solid State Nucl. Magn. Reson.*, 2017, **84**, 45.
16 K. J. Harris, A. Lupulescu, B. E. G. Lucier, L. Frydman and R. W. Schurko, *J. Magn. Reson.*, 2012, **224**, 38.
17 A. R. Altenhof, S. Wi and R. W. Schurko, *Magn. Reson. Chem.*, 2021, **59**, 1009.
18 J. J. Kimball, A. R. Altenhof, M. J. Jaroszewicz and R. W. Schurko, *J. Phys. Chem. A*, 2023, **127**, 9621.
19 S. Wi, Z. Gan, R. Schurko and L. Frydman, *J. Chem. Phys.*, 2015, **142**, 064201.
20 S. Wi, R. Schurko and L. Frydman, *J. Chem. Phys.*, 2017, **146**, 43.
21 S. Wi, R. W. Schurko and L. Frydman, *Solid State Nucl. Magn. Reson.*, 2018, **94**, 31.
22 D. Massiot, I. Farnan, N. Gautier, D. Trumeau, A. Trokiner and J. P. Coutures, *Solid State Nucl. Magn. Reson.*, 1995, **4**, 241.
23 I. Hung, A. J. Rossini and R. W. Schurko, *J. Phys. Chem. A*, 2004, **108**, 7112.
24 A. J. Pell, G. Pintacuda and L. Emsley, *J. Chem. Phys.*, 2011, **135**, 144201.
25 A. J. Pell, G. Kervern, L. Emsley, M. Deschamps, D. Massiot, P. J. Grandinetti and G. Pintacuda, *J. Chem. Phys.*, 2011, **134**, 1.
26 A. J. Pell, K. J. Sanders, S. Wegner, G. Pintacuda and C. P. Grey, *J. Chem. Phys.*, 2017, 146.
27 K. J. Sanders, A. J. Pell, S. Wegner, C. P. Grey and G. Pintacuda, *Chem. Phys. Lett.*, 2018, **697**, 29.
28 J. P. Carvalho and A. J. Pell, *J. Magn. Reson.*, 2021, **324**, 42.
29 J. S. Frye and G. E. Maciel, *J. Magn. Reson.*, 1982, **48**, 125.
30 H. J. Jakobsen, V. Langer, P. Daugaard and H. Bildsøe, A Device and Method for Magic-Angle Adjustment with Millidegree Accuracy using MAS of Quadrupolar Nuclei. In 31st Experimental NMR Conference, Asilomar, CA, 1990.
31 A. R. Altenhof, A. W. Lindquist, L. D. D. Foster, S. T. Holmes and R. W. Schurko, *J. Magn. Reson.*, 2019, **309**, 106612.
32 R. K. Harris, E. D. Becker, S. M. Cabral De Menezes, R. Goodfellow and P. Granger, *Concepts Magn. Reson.*, 2002, **14**, 326.
33 J. C. Edwards and P. D. Ellis, *Magn. Reson. Chem.*, 1990, **28**, S59.
34 A. R. Altenhof, M. J. Jaroszewicz, A. W. Lindquist, L. D. D. Foster, S. L. Veinberg and R. W. Schurko, *J. Phys. Chem. C*, 2020, **124**, 14730.
35 Y. Shrot and L. Frydman, *J. Magn. Reson.*, 2005, **172**, 179.
36 J. Koppe and M. R. Hansen, *J. Phys. Chem. A*, 2020, **124**, 4314.
37 R. Bhattacharyya and L. Frydman, *J. Chem. Phys.*, 2007, **127**, 194503.
38 F. H. Larsen, H. J. Jakobsen, P. D. Ellis and N. C. Nielsen, *J. Phys. Chem. A*, 1997, **101**, 8597.
39 M. Bak, J. T. Rasmussen and N. C. Nielsen, *J. Magn. Reson.*, 2000, **147**, 296.
40 J. Herzfeld and A. E. Berger, *J. Chem. Phys.*, 1980, **73**, 6021.
41 N. C. Nielsen and M. Bak, *J. Magn. Reson.*, 1997, **125**, 132.
42 M. W. Maciejewski, A. D. Schuyler, M. R. Gryk, I. I. Moraru, P. R. Romero, E. L. Ulrich, H. R. Eghbalnia, M. Livny, F. Delaglio and J. C. Hoch, *Biophys. J.*, 2017, **112**, 1529.
43 P. Caravatti, G. Bodenhausen and R. R. Ernst, *J. Magn. Reson.*, 1983, **55**, 88.
44 J. Baum, R. Tycko and A. Pines, *Phys. Rev. A: At., Mol., Opt. Phys.*, 1985, **32**, 3435.
45 E. O. Stejskal, J. Schaefer and J. S. Waugh, *J. Magn. Reson.*, 1977, **28**, 105.
46 M. Sardashti and G. E. Maciel, *J. Magn. Reson.*, 1987, **72**, 467.
47 I. Hung and Z. Gan, *J. Magn. Reson.*, 2015, **256**, 23.
48 X. Wu and K. W. Zilm, *J. Magn. Reson., Ser. A*, 1993, **104**, 154.
49 B. H. Meier, *Chem. Phys. Lett.*, 1992, **188**, 201.
50 Z. H. Gan and D. M. Grant, *Chem. Phys. Lett.*, 1990, **168**, 304.
51 J. Koppe, J. E. Frerichs and M. R. Hansen, *J. Phys. Chem. Lett.*, 2023, **14**, 10748.
52 M. Deschamps, Ultrafast Magic Angle Spinning Nuclear Magnetic Resonance, *Annual Reports on NMR Spectroscopy*, Elsevier Ltd, Amsterdam, 2014, vol. 81, pp. 109–144.

53 Y. Nishiyama, G. Hou, V. Agarwal, Y. Su and A. Ramamoorthy, *Chem. Rev.*, 2023, **123**, 918.
54 M. J. Jaroszewicz, L. Frydman and R. W. Schurko, *J. Phys. Chem. A*, 2017, **121**, 51.
55 P. Paluch, A. G. M. Rankin, J. Trébosc, O. Lafon and J. P. Amoureux, *Solid State Nucl. Magn. Reson.*, 2019, **100**, 11.
56 A. Venkatesh, F. A. Perras and A. J. Rossini, *J. Magn. Reson.*, 2021, **327**, 106983.
57 Z. Wang, L. A. Völker, T. C. Robinson, N. Kaeffer, G. Menzildjian, R. Jabbour, A. Venkatesh, D. Gajan, A. J. Rossini and C. Copéret, *et al.*, *J. Am. Chem. Soc.*, 2022, **144**, 21530.
58 M. J. Jaroszewicz, A. R. Altenhof, R. W. Schurko and L. Frydman, *J. Am. Chem. Soc.*, 2021, **143**, 19778.
59 B. E. G. Lucier, A. R. Reidel and R. W. Schurko, *Can. J. Chem.*, 2011, **89**, 919.
60 B. L. Phillips, J. R. Houston, J. Feng and W. H. Casey, *J. Am. Chem. Soc.*, 2006, **128**, 3912.
61 H. Harbor-Collins, M. Sabba, G. Moustafa, B. Legrady, M. Soundararajan, M. Leutzsch and M. H. Levitt, *J. Chem. Phys.*, 2023, **159**, 104307.
62 S. T. Holmes, J. Schönzart, A. B. Philips, J. J. Kimball, S. Termos, A. R. Altenhof, Y. Xu, C. A. O'Keefe, J. Autschbach and R. W. Schurko, *Chem. Sci.*, 2024, **15**, 2181.
63 B. A. Atterberry, P. Paluch, A. R. Lamkins, W. Huang and A. J. Rossini, *J. Am. Chem. Soc.*, 2025, **147**, 14411.
64 J. J. Kimball and R. W. Schurko, *J. Phys. Chem. Lett.*, 2025, **16**, 4596.

